RSC Advances

ROYAL SOCIETY OF CHEMISTRY

www.rsc.org/advances

RSC Advances

Dynamic Article Links ▶

ARTICLE TYPE

Novel Synergistic Combinations of Amphiphilic Fatty Acid Derivatives for High-Performance Rubber-Organoclay Nanocomposites

Dae Up Ahn,* Jun-Bae Jeon and Seong-Jin Kim

We report on the synergistic binary combination of amphiphilic fatty acids and their derivatives (FADs), remarkably enhancing the mechanical and thermal properties of crosslinked ethylene-propylene-diene monomer (EPDM)-organoclay nanocomposite as well as the melt processability of its non-crosslinked counterpart. The binary FAD mixture is composed of a stearic acid derivative (SAD) preferentially 10 increasing the gallery gap of organoclays and a vegetable oil mainly improving the dispersion of SAD-modified organoclays in the rubber matrix. The synergism between two FADs increases as both FAD components become more compatible with rubber matrix as long as the SAD component has a good affinity to organoclay enough to intercalate into its gallery and wet its surface. Such outstanding performance enhancement has been achieved even at a very low loading level of organoclay simply by 15 the incorporation of a suitable mixture of commercial-grade FADs during the traditional rubber compounding process. Therefore, we illustrate a novel and facile method to prepare a high-performance rubber nanocomposite with wide-ranging commercial benefits, without compromising the intrinsic advantages of rubber materials such as lightweight, optical transparency, high ductility and flexibility.

Introduction

20 A variety of micro-sized inorganic fillers have been incorporated into polymeric materials as a most cost-effective way to enhance their performance.[1,2] In general, a specific rubber performance increases with the amount of micro-sized filler until reaching to a threshold, and it often needs very high loading level of filler to 25 attain a satisfactory performance. However, the incorporation of large amount of filler necessarily accompanies a serious loss of intrinsic advantages of host rubber material, such as lightweight, excellent processability, optical transparency, high elasticity and flexibility.[2-5] In comparison to such conventional micro-sized 30 filler, the nano-filler can improve the rubber performance without compromising the intrinsic advantages because the same level of enhancement is achievable with much smaller amount of nano-filler. For the last few decades, therefore, numerous nano-fillers such as layered silicates, polyhedral oligomeric silsesquioxanes, 35 carbon nanotubes, graphines and nanosilicas have been extensively investigated for the fabrication of high-performance rubber materials maintaining their intrinsic advantages.[3-11]

Montmorillonite (MMT), which belongs to the 2:1 family of phyllosilicate clay minerals with a layered structure of c.a. 1 nm-40 thick silicate sheets, has been most frequently used for the fabrication of a rubber nanocomposite owing to its high commercial availability, low cost and high surface area.[11-13] Each crystal layer of MMT is composed of two silica tetrahedral layers linked to both sides to a central octahedral sheet of aluminum and 45 magnesium hydroxides. The isomorphous substitution of Al^{3+} by Mg^{2+} and Fe^{2+} in the octahedral sheet results in a net negative charge in the sandwiched layers, which is balanced with cations such as Na^+ and K^+ intercalated in the interlayer region (i.e., the gallery) of MMT. MMT can enhance a variety of physical and 50 chemical properties of a rubber, such as mechanical, barrier and oil properties as well as flame retardancy especially when well-dispersed in the rubber matrix. As usual, however, it is not an easy task to achieve a good dispersion of MMT particularly over a non-polar rubber matrix due to the polar nature of MMT, which 55 hinders the intercalation of rubber molecules into the MMT gallery and thus the dissociation of silicate sheets into individual layers (i.e., the exfoliation of MMT) in the rubber matrix. Furthermore, micrometer-scale MMT aggregates frequently evolve in a non-polar rubber matrix due to the preferential 60 interactions between MMTs, which behave more like conventional micro-sized fillers.

To overcome such difficulties, many researchers have modified the pristine MMT with amphiphilic organic molecules such as quaternary ammonium compounds with long 65 hydrophobic tails.[11,13-15] The organic molecules not only replace the intercalated cations but also reduce the surface polarity of MMT. Thus, the organic modification increases the gap distance between the layers and the affinity between MMT and rubber molecules at the same time, and consequently promotes the 70 intercalation of rubber molecules and the exfoliation of MMT layers as well as the MMT dispersion. In many cases, however, the performance of a crosslinked rubber was not remarkably improved in spite of the incorporation of an organically modified MMT (i.e., organoclay). This indicates that the organic 75 modification is not a sufficient step to produce a well-exfoliated

and dispersed MMT structure in a rubber matrix.[4]
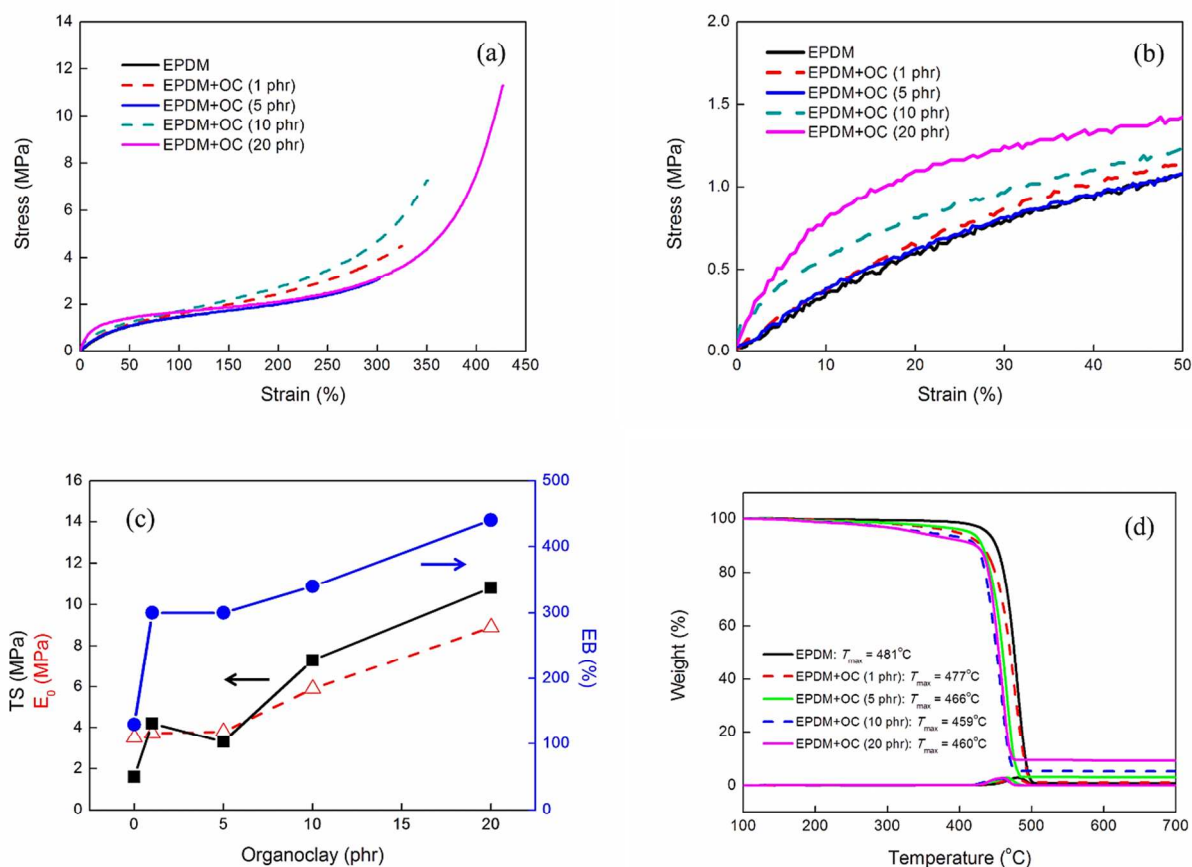
Fig. 1 Stress-strain curves (a and b) and TGA thermograms (d) of crosslinked EPDMs with different loading level of OC. The TS, EB and E_0 determined from the stress-strain curves were collected in (c).

Most of commercial rubber products contain various ingredients including curing agents, antioxidants, flame retardants, process aids, fillers and other organic/inorganic additives with special functionalities.[1] From a practical viewpoint, therefore, it is very important to understand the effects of such rubber ingredients on the intercalation, exfoliation and dispersion of organoclay in a rubber matrix. It has been reported that accelerators for sulfur vulcanization, like thiuram and dithiocarbamate, were able to facilitate the exfoliation process of organoclay in an ethylenepropylene-diene monomer (EPDM) rubber matrix by increasing the polarity of the rubber molecules.[16] The rubber molecules chemically modified by the accelerators intercalated more easily into the gallery gap owing to the hydrogen bonds between the polar groups of rubber and the silanol groups of organoclay. In addition, a silane coupling agent such as 3-(mercaptopropyl)trimethoxy silane enhanced the reinforcing ability of organoclay by forming both Si-O-Si coupling bonds with the hydroxyl groups of organoclay and Si-C coupling bonds with nitrile-butadiene rubber (NBR) molecules at the same time.[17] Furthermore, stearic acid frequently incorporated into various rubber products as a plasticizer, process aid, mold lubricant and/or activator also promoted the intercalation-exfoliation process of organoclay in the NBR matrix when a sulfur-curing package was used for the NBR vulcanization.[18] This was attributed to the easy intercalation of small stearic acid molecules into the gallery gap. Maleic anhydride-grafted EPDM (MA-g-EPDM) and epoxidized natural rubber (ENR) also facilitated the intercalation-exfoliation process of organoclay in EPDM and natural rubber (NR), respectively, by rendering the rubber chains polar.[19-22] However, we note that such compatibilizing methods above still require relatively high loading level of organoclay for a notable improvement of tensile strength (TS), which frequently accompanies the decrease in elongation at break (EB). For instance, in spite of the incorporation of MA-g-EPDM compatibilizer, the TS (or EB) of EPDM-organoclay exceeded neither 6 MPa (or 300%) at 5 phr (parts per one hundred parts of rubber) of organoclay nor 14 MPa (or 600%) at 15 phr of organoclay.[19]

In this study, we have engineered high-performance rubber-organoclay nanocomposites by incorporating a suitable binary mixture of amphiphilic fatty acids and their derivatives (FADs) widely used as additives in many fields of rubber industry. The binary FAD mixture has remarkably enhanced not only the melt processability of non-crosslinked rubber-organoclay nanocomposite but also the mechanical properties of its crosslinked counterpart, including TS, EB and modulus. Such outstanding reinforcement has been achieved at a loading level of organoclay below c.a. 5 phr. Therefore, our approach illustrated

here will provide great commercial advantages in engineering a high-performance rubber material.
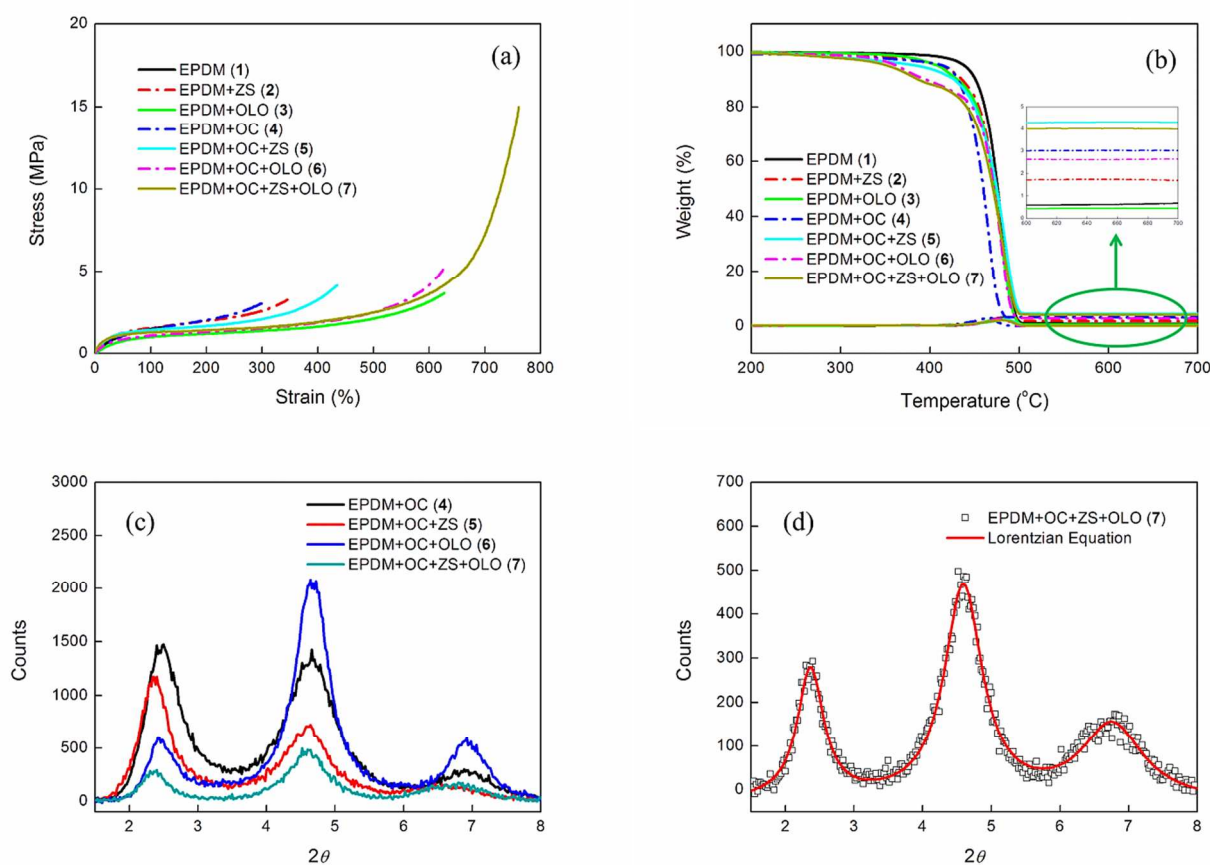
5 **Fig. 2** Stress-strain curves (a), TGA thermograms (b) and XRD patterns (c) of crosslinked EPDMs with OC, ZS and OLO of different combinations. (d) is the XRD pattern of **7** fitted with the Lorentzian equation for a 3-peak spectrum.

Results and Discussion

EPDM-Organoclay Nanocomposites Containing no FADs

Fig. 1 shows the mechanical and thermal properties of
10 crosslinked EPDMs containing different amounts of organoclay (Dellite 67G, OC). The modulus in the linear region (E_0) of each sample was determined from the slope of stress-strain curve in the region of strain from 0 to 10%, where the slope was almost linear as shown in Fig. 1(b). Thus, the E_0 will reasonably
15 correspond to the tensile modulus in the linear region, representing the stiffness of a sample. The TS, EB and E_0 of each sample, averaged from five different universal tensile testing machine (UTM) measurements, are also collectively depicted in Fig. 1(c).
20 As shown in Fig. 1, the ultimate mechanical properties of crosslinked EPDM such as TS and EB were considerably improved after loading 1 phr of organoclay, but the TS somewhat reduced at 5 phr while the EB remained constant. On the basis of the mechanical properties of unfilled EPDM (TS = 1.6 MPa and
25 EB = 130%), the degrees of increment in TS and EB per 1 phr of OC (ΔTS and ΔEB, respectively) were correspondingly 2.6 MPa/phr and 170%/phr at 1 phr, but 0.34 MPa/phr and 34%/phr at 5 phr. Above 5 phr, both TS and EB increased again as the

amount of organoclay increased, displaying ΔTS = 0.57 MPa/phr
30 and ΔEB = 21%/phr at 10 phr and ΔTS = 0.46 MPa/phr and ΔEB = 16%/phr at 20 phr. Meanwhile, the E_0 remained almost constant up to 5 phr but significantly increased from 3.8 to 8.9 MPa with increasing the amount of organoclay from 5 to 20 phr. Similarly, the minimum torque value (S_{min}) in a moving die rheometer
35 (MDR), representing the viscosity of uncrosslinked EPDM-OC nanocomposite, was also not much affected by the loading level of organoclay up to 5 phr (S_{min} of unfilled EPDM = 0.58 mN; S_{min} at 1 and 5 phr = 0.56 and 0.47 mN, respectively) but considerably increased as the loading level of OC increased from 5 to 20 phr
40 (S_{min} at 10 and 20 phr = 0.82 and 1.26 mN, respectively). Such experimental results indicate that, around the loading level of 1 phr, the organoclay somewhat behaves as a nano-sized reinforcing filler which significantly improves the ultimate mechanical properties of host polymer without significantly
45 affecting other intrinsic polymer properties including viscosity and modulus. Above c.a. 5 phr, however, the organoclay rather behaves as a conventional micro-sized reinforcing filler and quite alters the intrinsic polymer properties, which might be due to the micrometer-level aggregation of organoclay in the non-polar
50 EPDM matrix. In this study, to demonstrate the effectiveness of our FAD mixture more evidently, we have selected the EPDM-OC nanocomposite containing 5 phr of OC as a reference because

it rather behaves as a micro-composite and exhibits the lowest TS.

As shown in the Fig. 1(d), the temperature at which the maximum rate of weight loss occurred (T_{max}), determined from the maximum peak of the thermal derivative of thermogravimetric analysis (TGA) thermogram and representing the thermal stability of EPDM matrix, decreased from 481°C to 459°C with increasing the amount of OC from 0 to 10 phr. This is known to be arising from the hydroxyl groups on the edges of MMT layers, promoting the chain scission reactions of polymer matrix.[23,24] The T_{max} did not further decrease from 459°C although the loading level of OC increased from 10 phr to 20 phr, suggesting that the catalytic chain scission reaction due to OC should reach a threshold at c.a. 10 phr. The TGA results also showed that the weight of residue simply increased with the loading level of OC.

Table 1 Summary of MDR, UTM, TGA and XRD results of EPDMs with OC, ZS and OLO of different combinations.

Sample code	Formulation	S_{min} (mN)	TS (MPa)	EB (%)	E_0 (MPa)	T_{max} (°C)	$d_{(001)}$ (Å) Total Peak Area
1	EPDM PBP-98 (2 phr)	0.58	1.6	130	3.5	481	-
2	**1**+ZS (10 phr)	0.20	3.5	350	4.8	479	-
3	**1**+OLO (10 phr)	0.23	3.5	600	2.0	479	-
4	**1**+OC (5 phr)	0.47	3.3	300	3.8	466	35.3 4700
5	**4**+ZS (10 phr)	0.30	4.1 (5.2)[a]	440 (520)	5.1 (5.1)	485	37.2 2200
6	**4**+OLO (10 phr)	0.23	5.2 (5.2)	630 (770)	3.3 (2.3)	480	35.8 3000
7	**6**+ZS (10 phr)	0.26	14.8 (7.1)	770 (990)	6.0 (3.6)	482	37.8 1000

[a] The value expected by the additivity rule = Original value of **4** + the increment or decrement due to the FADs in the absence of OC.

EPDM-Organoclay Nanocomposites Containing FADs of Different Combinations

Fig. 2 shows the stress-strain curves (Fig. 2(a)) and TGA thermograms (Fig. 2(b)) of crosslinked EPDMs containing OC, zinc stearate (ZS) and olive oil (OLO) of different combinations as well as the wide-angle X-ray diffraction (XRD) patterns of their organoclay-containing counterparts (Fig. 2(c)). The TS, EB and E_0 of each sample, averaged from five different UTM tests, are also listed in Table 1 together with the S_{min}, T_{max} and $d_{(001)}$-spacing correspondingly obtained from the MDR, TGA and XRD measurements. The $d_{(001)}$-spacing of organoclay, representing the gallery gap between two parallel plates of organoclay, was calculated from the 2θ value at which the diffraction peak of (001) crystal surface reaches to the maximum. The total area of the three crystal surface peaks, inversely correlating with the degree of exfoliation of organoclay, was determined from the curve fitting of the XRD pattern with the Lorentzian equation for a 3-peak spectrum (Fig. 2(d)). For the quantitative comparison between the peak areas of different samples as precisely as possible, the sample thickness was maintained at 1.1±0.1 mm, and two X-ray scans were carried out on each sample at two different sample positions perpendicular to each other. For a given sample, both X-ray diffraction patterns recorded at two different sample positions were almost identical to each other, representing no preferred orientation of organoclay during the molding and crosslinking process.[4]

As shown in Table 1, the S_{min} of non-crosslinked EPDM significantly decreased after the addition of ZS and OLO, indicating that both behave as process aids to facilitate the melt flow of EPDM before its crosslinking. In comparison, both TS and EB of unfilled crosslinked EPDM (**1**) increased after the incorporation of ZS and OLO (Fig. 2(a) and Table 1). We can consider two different origins of such increment in ultimate mechanical properties: the reinforcing effects of the additives, which actually enhance the mechanical properties of a sample and the plasticizing effects of the additives, which merely span the range of elongational deformation without a significant loss of mechanical strength as identified especially at a low loading level of plasticizer compatible with rubber matrix. We note that the E_0 of ZS-containing EPDM (**2**) was larger than that of **1** and the incremental ratio of TS (i.e., TS of **2**/TS of **1** = 2.2) was similar to that of EB (i.e., EB of **2**/EB of **1** = 2.7). In contrast, the E_0 of OLO-containing EPDM (**3**) was smaller than that of **1** and the incremental ratio of TS (2.2) was much smaller than that of EB (4.6). Thus, we expect that, for the unfilled crosslinked EPDM, ZS rather behaves as a reinforcing additive while OLO as a plasticizer. It is noticeable that the process aid-like behaviour of ZS has changed to reinforcing additive-like during the crosslinking process since zinc activates the radical-driven crosslinking reaction. The thermal stability of EPDM was not much affected by the addition of the 10 phr of ZS and OLO, but the residue weight of ZS-containing EPDM was somewhat larger than those of unfilled and OLO-containing EPDMs as shown in the inset of Fig. 2(b) due to the zinc of ZS.

Upon incorporating 10 phr of ZS together with 5 phr of OC into the EPDM, the S_{min} of EPDM-OC nanocomposite (**4**) decreased from 0.47 to 0.30 mN (Table 1), indicating that ZS somewhat behaved as a process aid for **4** before its crosslinking. However, it is notable that the degree of decrement upon ZS incorporation (i.e., E_0 of **4** − E_0 of **5** = 0.17 mN) was smaller in comparison to the case of **1** that did not contain OC (i.e., E_0 of **1** − E_0 of **2** = 0.38 mN).
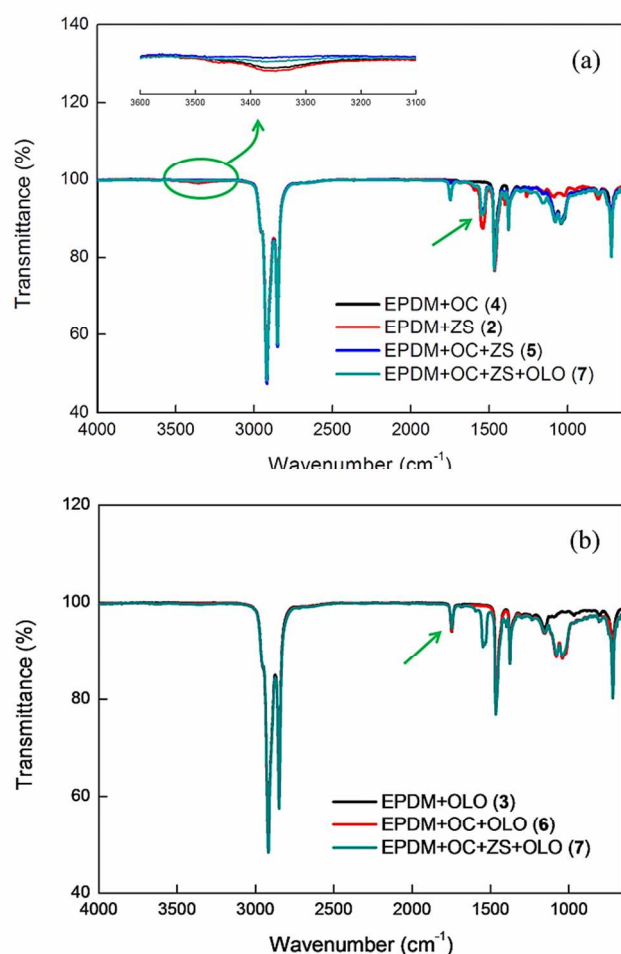
Fig. 3 IR spectra of crosslinked EPDMs with OC, ZS and OLO of different combinations.

5 This implies that there should be some interaction between OC and ZS, mitigating the original plasticizing efficiency of ZS. After crosslinking, the mechanical properties were improved in appearance in comparison to those of **4** as shown in Fig. 2(a) and Table 1. In addition, both the thermal stability of EPDM matrix
10 and the $d_{(001)}$-spacing (i.e., the gallery gap) of the organoclay also increased after the additional incorporation of ZS (Fig. 2(b) and (c)). Moreover, the total peak area of XRD pattern (i.e., the amount of organoclays maintaining their original layered crystal structure) also significantly decreased, representing the increase
15 of the amount of exfoliated organoclay. The enhancement of the thermal stability indicates that the ZS effectively suppresses the organoclay-catalyzed chain scission reaction of EPDM by scavenging the radicals arising from the homolysis of the –OH groups of organoclay at an elevated temperature. Such effective
20 protection of ZS confirms the presence of strong interactions between ZS and the –OH groups of OC. In addition, the increase in the $d_{(001)}$-spacing of OC also demonstrates the presence of strong interactions between ZS and the quaternary ammonium compound in the gallery of OC. Therefore, it is very clear that ZS
25 preferentially and strongly interacts with OC in physical and/or chemical manners. In spite of the interaction, however, we note that both TS and EB of 4.1 MPa and 440% are still less than

those predicted by simple additivity rule, 5.2 MPa and 520%, respectively (Table 1). This suggests that the interaction between
30 ZS and organoclay, which facilitates the intercalation-exfoliation process of organoclay, should adversely reduce the reinforcing efficiency of ZS, which enhances the mechanical properties of crosslinked EPDM by activating the crosslinking reaction as already identified in **2**.
35   To understand the behaviours of ZS and OLO in the presence of organoclay more clearly, we have performed infrared (IR) experiments on crosslinked EPDMs containing OC, ZS and OLO of different combinations. As shown in Fig. 3(a), the characteristic IR absorption peaks of ZS, appearing at c.a. 3360
40 cm^{-1} due to the –OH stretching and c.a. 1540 cm^{-1} due to the asymmetric stretching of –COO[-] group, were commonly identified in all ZS-containing EPDMs (**2**, **5** and **7**),[25] but their intensities (i.e., the amount of ZS in the EPDM matrix) significantly decreased in the presence of OC (**5** and **7**). Such IR
45 results indicate that considerable amount of ZS is preferentially consumed for being intercalated into the gallery gap of organoclay, which results in the depletion of ZS in the EPDM matrix and consequently reduces the ZS-driven reinforcement of EPDM. Thus, there will be a trade-off between the reinforcing
50 efficiencies of organoclay and ZS, inducing the increase of mechanical properties less than those predicted by the additivity rule, as identified in **5**. Meanwhile, the considerable decrease in the intensities of the IR absorption peaks due to the –OH and –COO[-] groups, as shown in **5** and **7**, represents again the presence
55 of strong interaction between ZS and OC. However, no new IR absorption peak arising from the evolution of a new chemical bond was identified in the IR spectra of the sample **5** and **7** even though both contained intercalated and exfoliated OC (i.e., ZS bound with the –OH groups and the quaternary ammonium
60 compound of OC) at the same time. Thus, we are currently expecting that the physical interactions, including ionic and polar interactions, should be more dominant between ZS and OC than their chemical reactions. However, still further detailed experiments are required to identify the type of interaction
65 between ZS and OC more clearly.
   After the addition of 10 phr of OLO together with 5 phr of organoclay, the S_{min} of **4** also decreased from 0.47 to 0.23 mN due to the plasticizing effect of OLO for non-crosslinked EPDM (Table 1). Similar to the case of ZS, however, the degree of
70 decrement upon OLO incorporating (i.e., E_0 of **4** – E_0 of **6** = 0.24 mN) was smaller in comparison to the case of **1** (i.e., E_0 of **1** – E_0 of **3** = 0.35 mN). This also indicates that there should be some interaction between OC and OLO, decreasing the original plasticizing efficiency of OLO. After crosslinking, the
75 mechanical properties were enhanced in comparison to those of **4** as shown in Fig. 2(a) and Table 1. The increased TS was mostly identical to that expected by simple additivity rule, 5.2 MPa while the EB of 630% was a little less than the expected value of 770%. Meanwhile, the E_0 synergistically increased to 3.3 MPa beyond
80 that expected by additivity rule, 2.3 MPa. Thus, the increase of TS is somewhat originated from the improved reinforcing efficiency of organoclay rather than the simple plasticizing effects of OLO (i.e., the increase of EB due to OLO). The thermal stability of EPDM matrix was also improved after the additional
85 incorporation of OLO in comparison to **4**, but a premature weight

loss of OLO was identified at c.a. 380°C, not observed in the absence of OC as shown in **3** (Fig. 2(b)). This TGA result represents that OLO, similar to ZS, also effectively suppresses the organoclay-promoted chain scission reaction of polymer matrix. Different from ZS directly relieving the catalytic reactivity of the –OH groups, however, OLO is preferentially extinguished with the functional groups at relatively lower temperature in advance of the thermal decomposition of EPDM matrix. The XRD and IR results of OLO-containing EPDM nanocomposite (**6**) were also distinguished from those of ZS-containing counterpart (**5**). The additional incorporation of OLO did not much enlarge the $d_{(001)}$-spacing of the organoclay (Fig. 2(c) and Table 1), and the characteristic IR absorption peak of OLO, appearing at c.a. 1745 cm^{-1} due to the C=O stretching, was almost invariant regardless of the presence of organoclay (Fig.

3(b)), indicating little involvement of OLO in the intercalation process of EPDM-organoclay nanocomposite (i.e., little interaction with the quaternary ammonium compound of OC). However, OLO still increased the degree of exfoliation (i.e., let the total peak area of XRD pattern decrease) to some extent even not as much as ZS did. From the experimental results above, therefore, we can expect that OLO mainly modifies the surface of organoclay, instead of being intercalated into the gallery gap. Consequently OLO will further promote the exfoliation-dispersion process of organoclay by facilitating the intercalation process of EPDM molecules into the gallery of organoclay. We note that the Hildebrand solubility parameter, δ of OLO (δ = 7.9 cal$^{1/2}$/cm$^{3/2}$)[26] is nearly identical to that of EPDM (δ = 7.9 cal$^{1/2}$/cm$^{3/2}$)[27], i.e., OLO is highly compatible with EPDM.
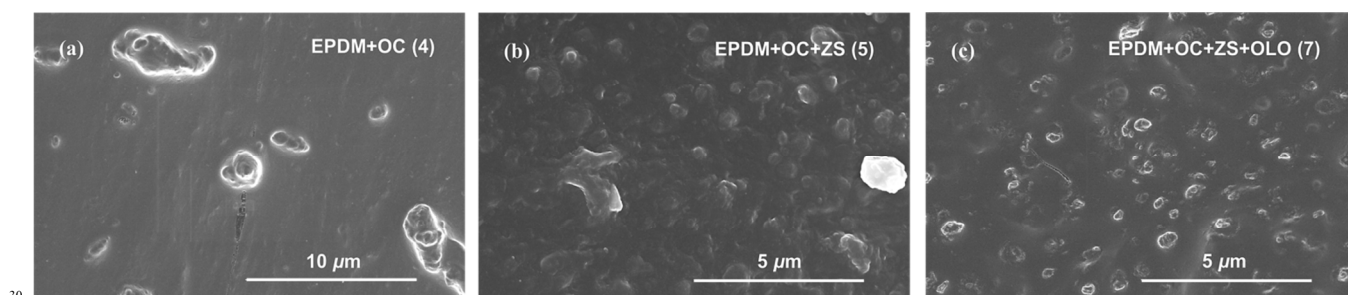

Fig. 4 FE-SEM images of crosslinked EPDM-OC nanocomposites with different combinations of ZS and OLO.

Our experimental results up to now reveal that both ZS and OLO preferentially behave as process aids for non-crosslinked EPDM-OC nanocomposite. For crosslinked one, in comparison, ZS mainly behaves as an organoclay-activating agent to facilitate the intercalation-exfoliation process of organoclay while OLO does as a dispersing agent to enhance mainly the degree of dispersion of organoclay in the EPDM matrix. Thus, we can predict an additional increase in melt processability and mechanical properties after the simultaneous incorporation of ZS and OLO together with organoclay as long as there is no serious antagonistic interaction among them. In addition to a considerable decrease in S_{min} as we expected, to our surprise, a remarkable enhancement of TS far exceeding that predicted by the additivity rule was experimentally identified after the addition of both ZS and OLO (Fig. 2(a) and Table 1). The TS reached as high as 14.8 MPa, 9.3 and 4.5 times higher than those of unfilled crosslinked EPDM (**1**) and EPDM-OC nanocomposite containing no dispersing agent (**4**), respectively. In addition, the E_0 also increased to 6.0 MPa far beyond that expected by the additivity rule, 3.6 MPa while the EB of 770% was less than the expected value of 990%. The decrease of S_{min} indicates that the mixture of ZS and OLO plays normal roles to increase the melt processability of non-crosslinked EPDM-organoclay nanocomposite as did each of them before. However, the dramatic increase of mechanical properties in **7** implies that there should be synergistic interactions between OC, ZS, OLO and/or EPDM, specially improving the reinforcing efficiency of OC. The origin of the synergism was envisaged from the additional TGA, XRD and IR experiments. Except for the weight of residue, the overall TGA thermogram of **7** was very similar to that of **6**, i.e., OLO increased the thermal stability of organoclay-containing EPDM by being extinguished with the catalytic functional groups

of organoclay prior to the thermal decomposition of EPDM matrix (Fig. 2(b)). This indicates that the way of interaction between OLO and organoclay is not much affected by ZS, i.e., the –OH functional groups, even if their catalytic reactivity for EPDM is relieved by ZS, still can promote the thermal decomposition of OLO, a sort of aliphatic esters. Meanwhile, the $d_{(001)}$-spacing of OC of **7** was not much different from that of ZS-containing EPDM-OC nanocomposite (**5**) as shown in Fig. 2(c) and Table 1, and the characteristic IR peaks of ZS (or OLO) of **7** were also almost identical with those of **5** (or **6**) as shown in Fig. 3(a) (or Fig. 3(b)). This confirms again that the way of interaction between OLO and organoclay is not much affected by ZS and vice versa, i.e., OLO (or ZS) behaves as a dispersing agent (or an organoclay-activating agent) for EPDM-OC nanocomposite (or organoclay) regardless of the presence of ZS (or OLO). Nevertheless, the total peak area of XRD pattern more markedly decreased after the simultaneous incorporation of ZS and OLO in comparison to the cases of **5** and **6** as shown in Fig. 2(c) and Table 1. Therefore, the synergism between two FADs with different functions, resulting in the dramatic increase of mechanical properties, should be originated from the additional increase in the degrees of exfoliation and dispersion of ZS-modified organoclays by the dispersing agent, OLO which further enhances the compatibility between EPDM and the ZS-modified organoclay.

Up to now, we have investigated not only the relatively small-scale morphology of OC embedded in the EPDM matrix (i.e., the degrees of intercalation and exfoliation) by using the XRD but also the larger-scale morphology of OC (i.e., the degree of dispersion) by measuring the bulk properties of rubber-organoclay nanocomposites, including mechanical and rheological properties. More direct information on the large-scale

OC morphology was also obtained from the field emission scanning electron microscopy (FE-SEM) experiments on the sample surfaces, fractured right after the sample quenching in the liquid nitrogen for several minutes. In the absence of FADs, micrometer-scale OC aggregates evolved in the EPDM matrix as shown in Figure 4(a) (**4**). In comparison, more homogeneous, much smaller and denser OC particles with the diameters somewhat less than 1 μm were developed over the whole sample area after the additional incorporation of ZS (**5**, Figure 4(b)). The overall size of the OC particles further decreased by submicrometer level after adding OLO to the ZS-containing EPDM-OC nanocomposite (**7**, Figure 4(c)). Such FE-SEM results clearly reveal that ZS (or OLO) greatly improves the dissociation and dispersion of organoclay aggregates (or ZS-modified organoclay aggregates) as well as the intercalation-exfoliation process of organoclay (or the exfoliation-dispersion process of the ZS-modified organoclay) as identified from the XRD results.

Effects of the Loading Level of FADs and Organoclay

To understand the role of each FAD more evidently, we have also investigated the changes in the mechanical and thermal properties of EPDM-OC nanocomposites upon varying the loading levels of OC, ZS and OLO (Fig. 5). At the given loading level of OLO (10 phr) and OC (5 phr), the S_{min} of non-crosslinked EPDM-OC nanocomposite increased after loading 5 phr of ZS (Fig. 5(a)) owing to its preferential interaction with the organoclay, which increasing the reinforcing efficiency of organoclay, in spite of the plasticizing effect of ZS for non-crosslinked EPDM matrix in the absence of OC as already confirmed in **2**.
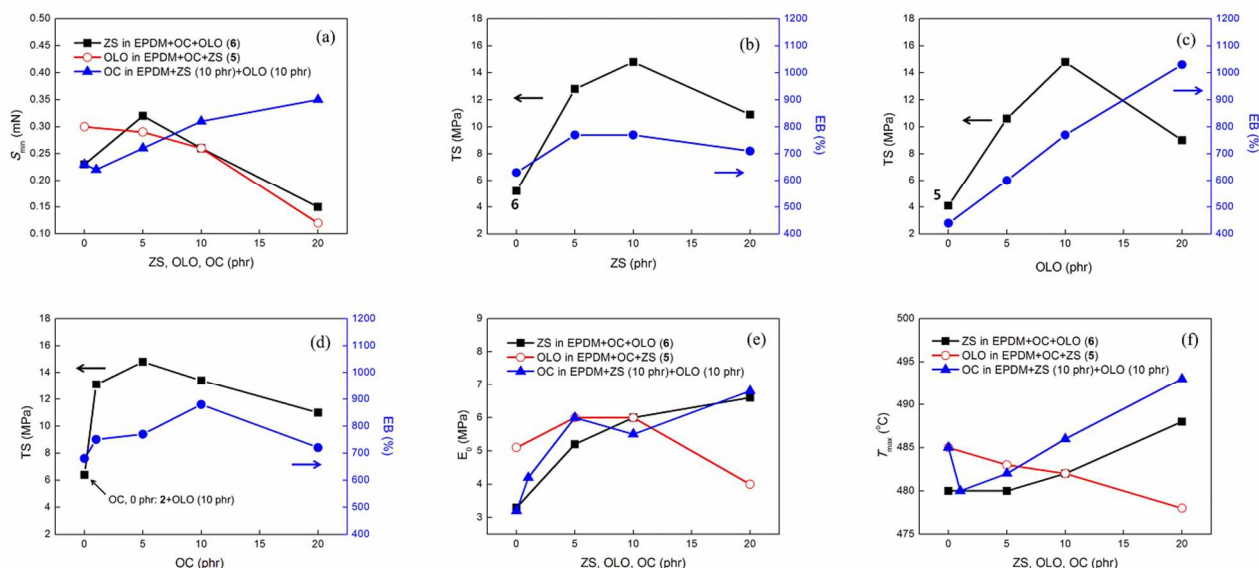
Fig 5 MDR (a), UTM (b – e) and TGA (f) results of EPDMs with OC, ZS and OLO of different combinations and loading levels.

As the loading level of ZS increased further, the S_{min} inversely decreased due to the increase of extra amount of ZS in the EPDM matrix, not interacting with the organoclay and thus behaving as a normal process aid for non-crosslinked EPDM. After the crosslinking process, in comparison, both TS and EB increased as the amount of ZS increased up to 10 phr but inversely decreased at 20 phr (Fig. 5(b)). Because the E_0 as well as the TS increased up to 10 phr (Fig. 5(e)), the increase of mechanical properties can be attributed to the enhanced reinforcing efficiency of OC by ZS. At the loading level of 20 phr, however, the decreases of TS and EB were accompanied with the increase of E_0. Thus, we expect that ZS remaining in the EPDM matrix after interacting with OC should increase the degree of crosslinking by activating the crosslinking reaction of EPDM. The thermal stability of EPDM-organoclay nanocomposite was not much changed up to 5 phr of ZS and then gradually increased with increasing the loading level of ZS to 20 phr as shown in Fig. 5(f). This indicates that the thermal stability increases with increasing both the amount of ZS-protected organoclay and the degree of crosslinking of EPDM matrix.

The S_{min} of the non-crosslinked EPDM-organoclay nanocomposite containing ZS (10 phr) and organoclay (5 phr) was slightly reduced with increasing the amount of OLO up to 10 phr and then more rapidly decreased at 20 phr (Fig. 5(a)). This indicates that OLO behaves as not only a process aid but also a dispersing agent for ZS-modified organoclays up to the loading level of 10 phr, while the excessive OLO does as a process aid at 20 phr. After the crosslinking process, both TS and E_0 reached to maximum values at around 10 phr while the EB continued to increase with increasing the loading level of OLO up to 20 phr (Fig. 5(c) and (e)). Thus, we expect that the role of OLO in the crosslinked EPDM-organoclay nanocomposite is not much different from that in the non-crosslinked counterpart because OLO is not significantly involved in the peroxide-driven crosslinking reaction of EPDM. The thermal stability of EPDM-organoclay nanocomposite gradually decreased with increasing the amount of low molecular weight organic compound, OLO (Fig. 5(f)).

At the given loading level of ZS (10 phr) and OLO (10 phr), the S_{min} of non-crosslinked EPDM increased as the loading level of organoclay increased from 1 to 20 phr, even though the 1 phr of OC did not much affect the S_{min} (Fig. 5(a)). The increase of

viscosity can be arising from not only the enhanced reinforcing efficiency of OC at nanoscopic level but also the increased amount of OC aggregates behaving mostly like micro-sized fillers. Thus, only from the result of S_{min}, it is hard to discern
5 which loading level of OC is nanoscopically most efficient at the given loading level of ZS and OLO. After the crosslinking process, in comparison, the TS notably increased with increasing the loading level of OC by 5 phr, accompanying a relatively small increment of EB, and then inversely decreased with increasing
10 the loading level of OC up to 20 phr (Fig. 5(d)). In addition, the E_0 also rapidly increased as the amount of loaded OC increased up to 5 phr but decreased at 10 phr (Fig. 5(e)). However, the E_0 increased again with increasing the loading level of OC further. Thus, we can conclude that, at the given loading level of ZS (10
15 phr) and OLO (10 phr), the OC behaves as a nano-filler below the

loading level of c.a. 5 phr, above which the characteristics of conventional micro-filler increase with the loading level of OC. We note that, after the simultaneous incorporation of ZS and OLO, the TS (or EB) of EPDM-OC nanocomposite has
20 surprisingly increased from 4.2 MPa (or 300%) to 13.1 MPa (750%) even at the loading level of OC as low as 1 phr (Fig. 1(c) and 5(d)), where the OC behaves as a real nano-filler. The thermal stability of EPDM-organoclay nanocomposite somewhat decreased after loading 1 phr of OC possibly due to the -OH
25 functional groups not yet inactivated by ZS but inversely increased with the amount of ZS-protected OC countervailing the influence of non-protected counterpart (Fig. 5(f)). It is worth mentioning that, at 20 phr of OC, the T_{max} markedly increased from 460°C to 493°C after the simultaneous incorporation of ZS
30 and OLO as shown in Fig. 1(d) and 5(f).

Table 2 Summary of MDR, UTM, TGA and XRD results of EPDMs with different FADs and organoclays.

Sample code	Formulation	S_{min} (mN)	TS (MPa)	EB (%)	E_0 (MPa)	T_{max} (^{o}C)	$d_{(001)}$ (Å)
8	**6**+SAmide (10 phr)	0.21	11.5 (3.5)[a]	800 (2.7)	4.0	482	53.5 (1.52)
9	**6**+SAcid (10 phr)	0.16	8.7 (2.6)	880 (2.9)	4.0	483	39.2 (1.11)
10	**5**+CCO (10 phr)	0.17	5.4 (1.6)	530 (1.8)	4.3	485	37.1 (1.05)
11	**1**+C30B (5 phr)	0.50	2.2	220	4.3	475	38.5
12	**11**+ZS (10 phr)+OLO (10 phr)	0.24	9.9 (4.5)	820 (3.7)	3.8	480	41.8 (1.09)

[a] The value in the parentheses = the value of EPDM-organoclay nanocomposite containing FADs / that of its counterpart containing no FADs.

Effective Binary Combinations of FADs and Effects of Organoclay Modifier

35 In this study, we have found that the mixture of two different FADs such as ZS and OLO can synergistically enhance the reinforcing efficiency of organoclay by increasing its degrees of intercalation, exfoliation and dispersion at the same time. At optimum loading levels, ZS, a stearic acid derivative (SAD),
40 behaved as an organoclay-activating agent improving the degrees of intercalation and exfoliation while OLO, a vegetable oil, did as a dispersing agent further increasing the degrees of exfoliation and dispersion of the SAD-modified organoclay. To further generalize our approach, we have also investigated the
45 effectiveness of other binary FAD mixtures: one was selected from SADs with different polar heads and the other from vegetable oils exhibiting different δ's (i.e., different affinities to organoclay and rubber matrix).

After the ZS of **7** was replaced with other SADs such as
50 stearamide (SAmide) and stearic acid (SAcid), the $d_{(001)}$-spacing (i.e., the degree of intercalation) of OC increased as shown in Table 2. If we consider the δ's of ZS, SAmide and SAcid are correspondingly 8.8, 9.7 and 9.4 cal$^{1/2}$/cm$^{3/2}$,[28] such increase of $d_{(001)}$-spacing should be arising from the enhanced polar
55 interaction of SAmide and SAcid with OC. Nevertheless, the TS and E_0 of crosslinked EPDM-OC nanocomposite as well as the viscosity (i.e., S_{min}) of its non-crosslinked counterpart a little decreased in comparison to **7**. This should be due to the poorer interactions of more polar SAmide and SAcid with relatively
60 non-polar OLO (δ = 7.9 cal$^{1/2}$/cm$^{3/2}$),[26] which deactivates the

following intercalation of EPDM molecules into the SAD-modified OC gallery and consequently reduces the degrees of exfoliation and dispersion of OC in the EPDM matrix. It is worth reminding that the mechanical properties of EPDM-organoclay
65 nanocomposites are significantly affected by their large-scale morphologies such as the degrees of filler aggregation and dispersion as identified in Fig. 4. From this experimental result, therefore, we expect that, to maximize the synergism of binary FAD mixture, the SAD should be compatible with the liquid-type
70 FAD component such as vegetable oil as much as possible within the limit of exhibiting a good interaction with organoclay enough to intercalate into its gallery and wet its surface. Nevertheless, it should be notable that both SAmide-OLO and SAcid-OLO combinations are still synergistic, considerably increasing the
75 ultimate mechanical properties of crosslinked EPDM-OC nanocomposite as well as the melt processability of non-crosslinked counterpart.

In comparison to the case of ZS, the replacement of OLO with other vegetable oils such as coconut oil (CCO) and castor oil
80 (CSO) more critically influenced on the mechanical properties of crosslinked EPDM-OC. As shown in Table 2, the mechanical properties more seriously decreased after the incorporation of CCO instead of OLO. Even more, CSO was too incompatible with EPDM to mix in a two roll mill. Considering the δ's of
85 OLO, CCO and CSO are correspondingly 7.9, 8.1 and 8.9 cal$^{1/2}$/cm$^{3/2}$,[26] we can expect that the liquid-type FAD component should be compatible with the rubber matrix for a synergistic FAD combination.

The FAD combination was also effective for other types of

organoclay modified with different organic compounds. The mechanical properties of crosslinked EPDM-organoclay also remarkably increased upon incorporating ZS and OLO at the same time regardless of the replacement of OC (an MMT modified with the less polar dimethyl dihydrogenated tallow ammonium salt) with C30B (an MMT modified with the more polar bis-2-hydroxyethyl methyl tallow ammonium salt) as shown in Table 2. The TS reached as high as 9.9 MPa, 7.2 and 4.5 times higher than those of unfilled crosslinked EPDM (**1**) and EPDM-C30B nanocomposite containing no amphiphilic FADs (**11**), respectively.

Experimental Section

Materials

A commercial-grade EPDM (KEP 510, Kumho Polychem Co., ethylene content = 71 wt.%, ethylidene norbornene content = 5.7 wt.%) was used as a base polymer. EPDM has been widely used as a key engineering material for tire, hose, seal, and cable insulation because it has a high insulation capability, low temperature flexibility, colour stability, and the ability to accommodate large quantities of oil as well as an excellent resistance to polar solvent.[29,30] Because of the non-polar character of EPDM, however, it is much more challenging to disperse organoclay well over EPDM matrix in comparison to other polar polymers.

Table 3 Ingredients and their compositions used for the fabrication of samples.

Ingredient[a] (Acronym)		Composition (phr)
Base polymer	EPDM	100
Organoclay	Dellite 67G (OC)	0 ~ 20
	Cloisite 30B (C30B)	
Stearic acid derivatives (SADs)	Zinc stearate (ZS)	0 ~ 20
	Stearamide (SAmide)	
	Stearic acid (SAcid)	
Vegetable oils	Olive oil (OLO)	0 ~ 20
	Coconut oil (CCO)	
	Castor oil (CSO)	

[a] The PBP-98 (2 phr) has been commonly incorporated to all samples as a curing agent.

Two commercial-grade MMTs treated with different organic modifiers were used for the fabrication of EPDM-organoclay nanocomposites: Dellite 67G, an MMT modified with the less polar dimethyl dihydrogenated tallow ammonium salt (Laviosa Chemica Mineraria S.p.A., $d_{(001)}$ = 3.48 nm) and Cloisite 30B, an MMT modified with the more polar bis-2-hydroxyethyl methyl tallow ammonium salt (Southern Clay Products Inc., $d_{(001)}$ = 1.85 nm).

To improve the intercalation, exfoliation and dispersion of organoclay in the rubber matrix, we have incorporated a variety of amphiphilic FADs with different δ's, which have been widely used in many fields of rubber industry as plasticizers, process aids, mold lubricants, accelerators and/or activators.[1,29] We divided the FADs into two categories for the sake of convenience; one is the stearic acid and its derivatives (SADs) with melting points higher than room temperature such as zinc stearate (Zn-st, Han-il Chem Co.), stearic acid (ST, LG Household & Healthcare) and stearamide (Finawax S, Fine Organics), the other is the vegetable oils with melting points lower than room temperature such as olive oil (a triglyceride mainly derived from oleic acid, linoleic acid, palmitic acid and stearic acid; CJ CheilJedang Co.), coconut oil (a triglyceride mainly derived from caproic acid, caprylic acid, capric acid, lauric acid and myristic acid; Lotte Food Ltd.) and castor oil (a triglyceride mainly derived from ricinoleic acid, oleic acid, linoleic acid, linolenic acid, stearic acid and palmitic acid; Dong Yang Oil Chemical).[31,32]

Bis(*t*-butylperoxyisopropyl)benzene (PBP-98, NOF Co.) was commonly incorporated to all EPDM-based samples as a curing agent. All materials used in this study were used as received.

Preparation of EPDM-Organoclay Nanocomposites

EPDM-organoclay nanocomposites and their unfilled counterparts were prepared on a traditional open two-roll mixing mill. Ingredients and their compositions used for the sample preparation are summarized in Table 3. EPDM base polymer was first pre-deformed in the roll mill for c.a. 3 min, and then predetermined amount of additives except for the curing agent were mixed with the base polymer at 60°C for c.a. 20 min. After the roll mill cooled to room temperature, the curing agent was added and mixed for another 20 min to prepare a non-crosslinked EPDM compound. Before curing, the optimum curing time of each sample was determined from the measurement of the time required to reach to 90% of the maximum torque (t_{c90}) in a moving die rheometer (MDR, MDR 2000, Alpha Technology). The compound then cured in a compression mold (pressure = 12.5 MPa) at 170°C and cooled to room temperature, and then kept for 1 day before doing any further testing.

Instrumental analysis

In addition to the optimum curing time, the melt processability of a non-crosslinked EPDM compound was also estimated from the measurement of minimum torque value (S_{min}) in an MDR. At a given temperature, the sample processability will increase with decreasing the S_{min} that directly correlates to the viscosity. For MDR measurements, a sinusoidal strain of 5% with amplitude of 0.5° and a frequency of 1.67 Hz were applied.

Tensile properties of crosslinked EPDM samples, such as TS, EB and E_0 were determined with a universal tensile testing machine (UTM, H10KS, Tiniusolsen). The mechanical tests were carried out on dumbbell-shaped samples (DIN 53504.S2) in uniaxial tension mode at a constant crosshead speed of 254 mm/min (IEC 60811-1-1). Five tests were performed on each sample, and the average values were used in this study.

The thermogravimetric analysis (TGA) was carried out on a TGA Q50 (TA Instrument) at a heating rate of 20°C/min under nitrogen atmosphere. In each case, c.a. 10 mg sample was examined in the range from ambient temperature to 800°C.

The $d_{(001)}$-spacing of organoclay in the EPDM matrix was determined from the wide-angle X-ray diffraction (XRD) measurements by using a Scintag XDS 2000 with CuKa radiation (40 kV and 40 mA) at a wavelength of 1.5406Å. The scanning 2θ
[5] angles ranged between 1 and 10° with a step-scanning rate of 1°/min. The $d_{(001)}$-spacing was calculated from Bragg's equation, $\lambda = 2d_{(001)}\sin\theta$ where λ is the wavelength of the X-ray, $d_{(001)}$ is the interlayer distance and θ is the angle of incident X-ray radiation.

The relatively large-scale morphology of organoclay
[10] embedded in the EPDM matrix was obtained from a field emission scanning electron microscope (FE-SEM, Magellan 400, FEI Co.). The FE-SEM experiments were carried out on the sample surfaces, fractured right after the sample quenching in the liquid nitrogen for several minutes and then coated with osmium.

[15] The infrared (IR) spectra of crosslinked EPDMs were recorded on a Fourier transform infrared spectroscope (FTIR, Nicolet IS10, Thermo Scientific) using the mode of attenuated total reflection (ATR).

Conclusions

[20] In this study, we have markedly enhanced the mechanical and thermal properties of crosslinked EPDM-organoclay nanocomposite as well as the melt processability of its non-crosslinked counterpart by incorporating a suitable mixture of two amphiphilic FADs, SAD and vegetable oil. The SAD
[25] behaves as an organoclay-activating agent to facilitate the intercalation-exfoliation process of organoclay while the vegetable oil does as a dispersing agent to promote the exfoliation-dispersion process of the SAD-modified organoclay. Such highly functional FAD mixture has been collected from the
[30] organic additives widely used in many fields of rubber industry, and compounded with EPDM and organoclay in a traditional open two roll mill at a relatively low temperature. In spite of the application of such highly commercialized materials and mixing process, an outstanding performance improvement has been
[35] achieved at a low loading level of organoclay below around 5 phr regardless of the type of intercalated organic modifier. Therefore, our novel FAD combination technique presented here will create great commercial advantages for the fabrication of a high-performance rubber nanocomposite that retains the intrinsic
[40] advantages of rubber materials such as lightweight, optical transparency, high ductility and flexibility.

Notes and references

Nexans Research Center, Nexans, 370-95, Yongjeong, Jincheon, Chungbuk, 365-853, Republic of Korea. Fax: +82 43 530 2144; Tel: +82
[45] *43 530 2130; E-mail: Dae-Up.AHN@nexans.com*

1   J. B. Horn, in *Rubber Technology and Manufacture* (Eds: C. M. Blow and C. Hepburn), Butterworth Scientific, London, 1982, Ch.6.
2   J.-B. Donnet and E. Custodero, in *Science and Technology of Rubber* (Eds: J. E. Mark, B. Erman and F. R. Eirich), Elsevier Academic
[50] Press, New York, 2005, Ch. 8.
3   P. Kiliaris and C. D. Papaspyrides, *Prog. Polym. Sci.*, 2010, **35**, 902.
4   A. Das, D.-Y. Wang, K. W. Stöckelhuber, R. Jurk, J. Fritzsche, M. Klüppel and G. Heinrich, *Adv. Polym. Sci.*, 2011, **239**, 85.
5   S. Bourbigot and S. Duquesne, *J. Mater. Chem.*, 2007, **17**, 2283.
[55] 6   Y. Kojima, A. Usuki, M. Kawasumi, A. Okada, Y. Fukushima, T. Kurauchi and O. Kamigaito, *J. Mater. Res.*, 1993, **8**, 1185.
7   S.-W. Kuo and F.-C. Chang, *Prog. Polym. Sci.*, 2011, **36**, 1649.
8   F. Hussain, M. Hojjati, M. Okamoto and R. E. Gorga, *J. Comp. Mater.*, 2006, **40**, 1511.
[60] 9   M. Endo, T. Noguchi, M. Ito, K. Takeuchi, T. Hayashi, Y. A. Kim, T. Wanibuchi, H. Jinnai, M. Terrones and M. S. Dresselhaus, *Adv. Funct. Mater.*, 2008, **18**, 3403.
10 X. Bai, C. Y. Wan, Y. Zhang and Y. H. Zhai, *Carbon*, 2011, **49**, 1608.
[65] 11 F. Bergaya and M. Jaber, in *Rubber Clay Nanocomposites – Science, Technology and Applications* (Ed: M. Galimberti), Wiley and Sons, New York, 2011, Ch. 2.
12 H. van Olphen, *An Introduction to Clay Colloid Chemistry*, Interscience, New York, 1963.
[70] 13 D. R. Paul and L. M. Robeson, *Polymer*, 2008, **49**, 3187.
14 P. C. LeBaron, Z. Wang and T. J. Pinnavaia, *Appl. Clay Sci.*, 1999, **15**, 11.
15 W. Xie, Z. Gao, W.-P. Pan, D. Hunter, A. Singh and R. Vaia. *Chem. Mater.*, 2001, **13**, 2979.
[75] 16 A. Usuki, A. Tukigase and M. Kato, *Polymer*, 2002, **43**, 2185.
17 J.-T. Kim, D.-Y. Lee, T.-S. Oh and D.-H. Lee, *J. Appl. Polym. Sci.*, 2003, **89**, 2633.
18 A. Das, R. Jurk, K. W. Stöckelhuber and G. Heinrich, *Macromol. Mater. Eng.*, 2008, **293**, 479.
[80] 19 K. G. Gatos and J. Karger-Kocsis, *Polymer*, 2005, **46**, 3069.
20 K. G. Gatos, A. A. Apostolov and J. Karger-Kocsis, *Mater. Sci. Forum*, 2005, **482**, 347.
21 S. Varghese, J. Karger-Kocsis and K. G. Gatos, *Polymer*, 2003, **44**, 3977.
[85] 22 J. Sharif, W. M. Z. W. Yunus, K. H. Dahlan and M. H. Ahmad, *J. Appl. Polym. Sci.*, 2006, **100**, 353.
23 M. Zanetti and L. Costa, *Polymer*, 2004, **45**, 4367.
24 M. C. Costache, D. D. Jiang and C. A. Wilkie, *Polymer*, 2005, **46**, 6947.
[90] 25 K.Volka, Z.Vymazal, J. Stavek and V. Seidl, *Eur. Polym. J.*, 1982, **18**, 219.
26 C. D. Vaughan, *J. Soc. Cosmet. Chem.*, 1985, **36**, 319.
27 P. C. Painter and M. M. Coleman, *Fundamentals of Polymer Science: An Introductory Text*, CRC Press, Florida, 1997.
[95] 28 R. F. Grossman, in *Polymer Modifiers and Additives* (Eds: J. T. Lutz Jr. and R. F. Grossman), Marcel Dekker, New York, 2001, Ch. 9.
29 P. A. Ciullo and N. Hewitt, *The Rubber Formulary*, Noyes Publications, New York, 2003.
30 C. Nah, J. Oh, B. Mensah, K.-U. Jeong, D. U. Ahn, S.-J. Kim, Y. Lee
[100] and S.-H. Nam, *J. Appl. Polym. Sci.*, 2015, **132**, 41324.
31 T. P. Pantzaris, Y. Basiron and D. Boskou, in *Vegetable Oils in Food Technology: Composition, Properties and Uses* (Ed: F. D. Gunstone), Blackwell Publishing, Oxford, 2002, Ch. 6 & 9.
32 M. M. Conceicao, R. A. Candeia, F. C. Silva, A. F. Bezerra, V. J.
[105] Fernandes Jr. and A. G. Souza, *Renewable and Sustainable Energy Reviews*, 2007, **11**, 964.

Table of Contents

Synergistic binary combinations of fatty acid derivatives have remarkably enhanced the performance of a rubber-organoclay nanocomposite.